PDMS free-flow electrophoresis chips with integrated partitioning bars for bubble segregation†‡

Stefan Köhler,[a] Claudia Weilbeer,[a] Steffen Howitz,[b] Holger Becker,[c] Volker Beushausen[d] and Detlev Belder*[a]

Received 27th August 2010, Accepted 15th October 2010
DOI: 10.1039/c0lc00347f

In this work, a microfluidic free-flow electrophoresis device with a novel approach for preventing gas bubbles from entering the separation area is presented. This is achieved by integrating partitioning bars to reduce the channel depth between electrode channels and separation chamber in order to obtain electrical contact and simultaneously prevent bubbles from entering the separation area. The three-layer sandwich chip features a reusable carrier plate with integrated ports for fluidic connection combined with a softlithographically cast microfluidic PDMS layer and a sealing glass slide. This design allows for a straightforward and rapid chip prototyping process. The performance of the device is demonstrated by free-flow zone electrophoretic separations of fluorescent dye mixtures as well as by the separation of labeled amines and amino acids with separation voltages up to 297 V.

Introduction

Micro free-flow electrophoresis (μFFE) is an attractive miniaturized separation technique which allows high speed continuous separations with a minimal sample amount.[1,2] Combined with an online detection technique μFFE has great potential as a portable analytical device *e.g.* for point of care diagnostics. The ability to perform micropreparative separations additionally facilitates the realization of complex lab-on-a-chip devices, integrating multistep chemical reactions, micropreparative separations and analysis on a single device.[3–7] Although the miniaturized versions of free-flow electrophoresis have several advantages over their macroscopic counterpart,[8] such as enhanced analysis speed, minimized sample and reagent consumption and efficient joule heat dissipation, there are also technical difficulties to overcome. One of the main challenges is the effective electrical connection between the electrodes and the separation region. For reliable μFFE operation it is essential to prevent generated electrolysis products, especially gas bubbles, from entering the separation area. In conventional macroscopic FFE devices this problem can rather easily be circumvented by manual integration of ion-permeable barriers like cellulose nitrate membranes in between electrode channels and the separation chamber.[9] An analogous manual implementation of similar membranes into microfluidic devices is, however, hardly applicable.

The first miniaturized free-flow electrophoresis device, introduced by Raymond *et al.*, used compact arrays of fine parallel side channels for separating the electrode and separation region. With this approach miniaturized zone electrophoresis as well as isotachophoresis in free-flow mode was realized.[10–15] A challenge in this layout is the rather high potential drop over the connecting side channels resulting in reduced effective electrical field strengths.

Kohlheyer *et al.* as well as Albrecht *et al.* implemented ion-permeable acryl amide membranes into μFFE chips for separating the separation and the electrode area.[16–19] With this approach bubbles were effectively hindered from entering the separation chamber and excellent results were obtained in free-flow zone electrophoresis and free-flow isoelectric focusing. A challenge in this design is, however, the limited chemical and mechanical stability of the membranes.

Fonslow *et al.* introduced a μFFE design with an open connection between electrode region and separation area which results in a remarkable voltage efficiency.[20–22] Due to the almost four times deeper electrode channels compared to the separation chamber an approximately 15 times higher linear buffer velocity could be applied in the electrode channels. This helped in removing bubbles while ensuring an effective electrical connection. A challenge in this device is the need for a very precise flow control to gain undistorted separations.

Another approach for bubble removal utilizing narrow banks between separation chamber and electrode region was demonstrated by Kobayashi *et al.*[23] In their device they continuously fractionated myoglobin and cytochrome C with high voltage efficiency.

Recently Song *et al.* published another method for creating a salt bridge in μFFE PDMS devices by a printed hydrophobic layer creating rupture points which act as junctions for the electrical connection between electrode and separation region.[24] With this device peptides and proteins could be separated successfully.

[a]*Institute of Analytical Chemistry, University of Leipzig, Linnéstr. 3, 04103 Leipzig, Germany. E-mail: belder@uni-leipzig.de*
[b]*GeSiM mbH, Bautzner Landstrasse 45, 01454 Grosserkmannsdorf, Germany*
[c]*Microfluidic ChipShop GmbH, Carl-Zeiss-Promenade 10, 07745 Jena, Germany*
[d]*Laser-Laboratorium Göttingen e.V., Hans-Adolf-Krebs-Weg 1, 37077 Göttingen, Germany*

† Electronic supplementary information (ESI) available: Free-flow zone electrophoretic separation of rhodamine 116, fluorescein and rhodamine 6G. See DOI: 10.1039/c0lc00347f

‡ Our work is dedicated to the memory of Volker Beushausen who passed away during the course of this project.

An unusual way for solving the bubble problem was demonstrated by Janasek *et al.* in 2006 showing μFFE with electrostatic induction.[25]

The highest voltage efficiency is of course achieved when the electrodes are directly located in the separation area. With this straightforward approach bubble formation can be minimized by either utilizing low voltages[26] and high flow rates[27] or by elegant electrochemical suppression of bubble formation.[28]

In this work we present a new straightforward μFFE design ensuring both, bubble free electrophoretic separation and effective electrical connection by implementing miniaturized partitioning bars. Thereby, defined open gaps of 10 μm in height and 50 μm in width are created between the electrode channels and the separation chamber. The design has been successfully realized in a PDMS glass device using a polycarbonate carrier plate with integrated ports for fluidic and electric connection.

Experimental

Materials and reagents

Rhodamine 116, rhodamine B, rhodamine 6G, (*S*)-2-butylamine, glycine, fluorescein-5-isothiocyanate (FITC, isomer I), 2-(cyclohexylamino)ethanesulfonic acid (CHES), 4-(2-hydroxyethyl)piperazine-1-ethanesulfonic acid (HEPES), polyvinylpyrrolidone (PVP), (hydroxypropyl)methylcellulose (HPMC), Tween 20, 1-propanol and 1-hexadecanethiol were purchased from Sigma-Aldrich-Fluka, L-aspartic acid and methanol were from Merck. Fluorescein (sodium salt) was purchased from Roth, Sylgard silicone base and curing agent for chip fabrication was from Dow Corning. Stock solutions of 3 mg ml^{-1} rhodamine 116, rhodamine B, rhodamine 6G and fluorescein were prepared in demineralized water. 2-Butylamine, 2-octylamine, glycine and aspartic acid stock solutions were labeled with FITC as described previously.[29] In order to avoid air bubbles the sample and buffer solutions were degassed in vacuum.

Chip fabrication

The three-layer chip design is based on the MicCell platform (GeSiM, Germany).[30] One layer consists of a polycarbonate carrier plate which provides for the connection to the fluidic channels and the electrodes. The intermediate PDMS layer, containing the microfluidic structure, is sealed to the carrier plate during the curing process and a glass slide with sputtered electrodes is used as a lid.

The manufacturing process as depicted in Fig. 1 was executed as follows: in a casting station the polycarbonate carrier plate was placed above a silicon master with the negative structure. The PDMS layer, containing the microfluidic structure, was formed by casting the polymer against a silicon master or a respective PDMS replicate.[31] Therefore, the remaining gap in between is filled with a degassed liquid mixture of silicone base and curing agent (10 : 1). After curing for two hours at 75 °C a 2-layer device consisting of a cured PDMS layer attached to the carrier plate is removed from the casting station.

In order to ensure a reliable sealing of the microfluidic structure with a glass slide including sputtered electrodes some additional experimental steps were found to be necessary. In order to enable bonding between gold and PDMS, 1-hexadecanethiol was used as adhesion promoter. For this purpose, the gold electrodes were treated with a solution of 0.001% 1-hexadecanethiol in 1-propanol and stored overnight under 1-propanol saturated atmosphere. Afterwards the glass slides were rinsed with 1-propanol, followed by deionized water. In order to avoid collapsing of the wide separation chamber and especially to prevent gluing of the partitioning bars to the glass slide, during the bonding step sodium chloride powder was deposited on top of the fluidic structure as release agent. Using a low pressure nitrogen plasma the PDMS layer and the electrode glass slide were permanently bonded. Thereafter, the three layered chip is rinsed with deionized water for several minutes to dissolve and remove the release agent sodium chloride.

The resulting chips are 50 mm × 75 mm in size with a thickness of 11 mm. The channel and chamber depth in the 25 mm × 75 mm PDMS layer is 50 μm, except for the partitioning bar space with a channel depth of 10 μm. Inlet and outlet channels are 200 μm wide. The width of the separation area is 2.8 mm while the electrode channels were 1 mm wide. The partitioning bars are each 50 μm wide. The length of the separation area as well as the electrode channels and partitioning bars is 11 mm.

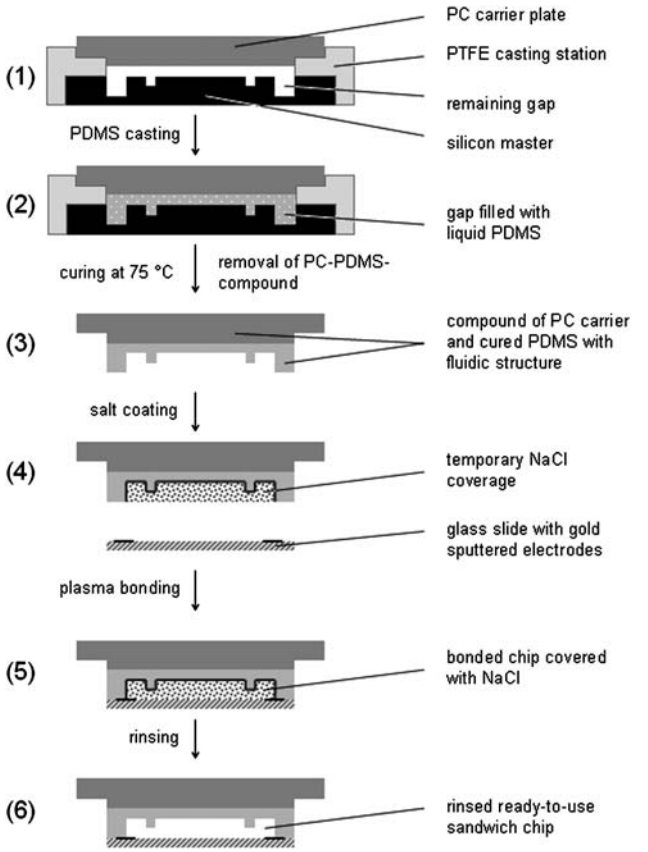

Fig. 1 Chip fabrication procedure. (1) Silicon master and polycarbonate carrier plate are placed in PTFE casting station. (2) Filling of remaining gap with PDMS base and curing agent. (3) Removal of carrier plate with PDMS layer containing microfluidic structure after curing at 75 °C. (4) Covering of the microfluidic structure with NaCl powder. (5) Plasma-bonding of PDMS layer and electrode glass slide. (6) Removal of salt coverage by rinsing with deionised water.

Experimental setup

The fabricated chips were connected to syringe pumps using polytetrafluorethylene capillary tubes (Supelco, USA) and standard flangeless fittings and ferrules (Upchurch Scientific, USA). The separation area inlets were connected to a pulsation free three channel syringe pump (Nemesys, cetoni, Germany). For the electrode channels a PHD 2000 syringe pump (Harvard Apparatus, USA) was used. All pumps were equipped with high precision glass syringes (ILS, Germany). Two custom-made PEEK screws with integrated gold contacts were used for the connection of the chip electrodes to the high voltage power supply (HCL 35-6500, FuG Elektronik, Germany). Photographs of a chip with and without fluidic connections are shown in Fig. 2a and b. The experimental setup includes a fluorescence microscope (Olympus IX71) equipped with a mercury burner and filter sets for FITC-labeled analytes (U-MWB2, Olympus) and multi-color fluorescent dyes (FITC/Cy3/Cy5, LOT-Oriel, Germany). A digital camera attached to the microscope (Panasonic NV-GS400) was used for monitoring and recording purposes.

During operation the sample solution was injected into the separation chamber through the center inlet and hydrodynamically focused by buffer flows from the adjacent inlets. The fluorescent dyes were separated using electrolytes consisting of 10 mM HEPES (pH 7.5), 0.2% HPMC and 0.1% Tween 20 in demineralized water or in aqueous methanol (50% v/v). The FITC-labeled analytes were separated in aqueous electrolytes consisting of 20 mM CHES (pH 8) with 0.2% HPMC and 0.1% Tween 20.

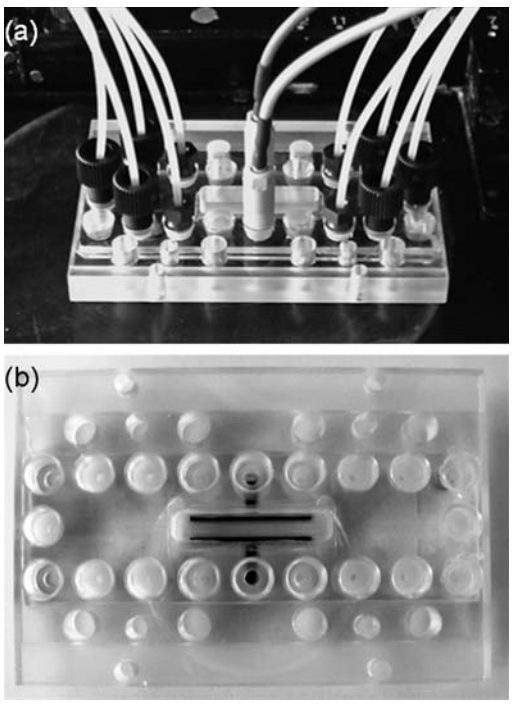

Fig. 2 FFE chips. (a) Fully connected chip placed on a fluorescence microscope. (b) Topview of an unconnected chip showing connection ports and electrode structure.

The following sample solutions were utilized. The aqueous dye test mixtures contained 100 μg ml^{-1} fluorescein, 400 μg ml^{-1} rhodamine 116 and 400 μg ml^{-1} rhodamine 6G. A test mixture containing 300 μg ml^{-1} fluorescein, rhodamine B and rhodamine 6G was used to determine the electrophoretic mobilities. For the separation of FITC-labeled analytes, sample solutions containing FITC–2-butylamine, FITC–2-octylamine, FITC–aspartic acid and FITC–glycine with varying composition and concentration were prepared in demineralized water. The structures of the sample molecules and their respective charges at experimental conditions are given in Fig. 3.

Electrophoretic mobilities μ were calculated using the migration distance d_M, the respective residence time t and the applied electrical field strength E

$$\mu = d_M t^{-1} E^{-1}. \quad (1)$$

Electrical field strengths were determined with the applied voltage U, the voltage efficiency η and the distance between electrodes d_E

$$E = \eta U d_E^{-1}. \quad (2)$$

Residence times are calculated from the buffer's linear velocity and the distance from the inlet to the detection point. The migration distance of fluorescein was determined using the neutral rhodamine B band as reference.

Results and discussion

The new chip layout was designed in order to hinder bubbles generated in the electrode channels from entering the separation channel while maintaining a good electrical connection. This is realized with an open gap at the bottom of the chip which is formed by partitioning bars in between the separation chamber

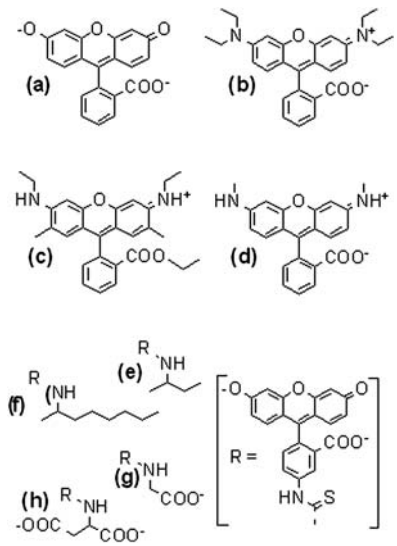

Fig. 3 Sample molecules and their respective charges under experimental conditions: (a) fluorescein, (b) rhodamine B, (c) rhodamine 6G, (d) rhodamine 116, (e) FITC–2-butylamine, (f) FITC–2-octylamine, (g) FITC–glycine, and (h) FITC–aspartic acid.

and the electrolyte channels. The design and working principle are schematically shown in Fig. 4.

The bars reduce the channel depth from 50 μm to 10 μm along the whole separation chamber length. Since the open fluidic junction between separation chamber and electrode channels is arranged at the chip bottom, gas bubbles should ascend to the topside where they are easily flushed out by the electrode buffer. This should effectively prevent interaction of bubbles with the separation process.

At the beginning of each experiment, buffer and sample flows were adjusted to form a narrow linear sample band. As soon as the electrical field is applied, the single sample band is split into individual analyte zones as expected. Furthermore, the generated bubbles were indeed ascending to the top of the electrolyte channels and flushed out by the electrode buffer stream as predicted. Only at high electrical currents utilizing high buffer concentrations and high electrical field strengths, a strong bubble formation was observed which can exceed the gas removal capacity of the electrode buffer streams. On these occasions, the electrode reservoirs can be filled almost completely with gas and bubbles can be forced into the separation chamber through the bottom gap. However, using suitable low conductivity buffers, adequate electrolyte flow velocities and by restricting the electrical current below 300 μA, separations of good long-term stability can be achieved. Due to the high stability of the μFFE process a directed hydrodynamic steering of separated bands to individual outlets was possible by adjusting the flow rates of the adjacent fluid streams.

In addition to the good performance of the device for bubble free operation, the design enables a high voltage efficiency which is a measure of how effective the electrical field is coupled into the separation process. The marginal width of the partitioning bars creating an open gap leads to only minor increase of electric resistance resulting in a voltage efficiency of almost 91%.

It is well known that it is challenging to fill PDMS chips with aqueous solutions in a bubble free manner due to the hydrophobic nature of PDMS. Wetting with aqueous solution can be improved by the addition of Tween 20 to the running buffer. A further significant improvement in bubble free filling with aqueous solutions was achieved by dynamically coating the inner channel surfaces with HPMC or PVP. These dynamic coatings also result in a reliably suppressed electroosmotic flow.

The performance of the device in free-flow zone electrophoresis could be successfully demonstrated by the separation of fluorescent dyes. An exemplary separation of fluorescein, rhodamine B and rhodamine 6G is shown in Fig. 5. For these experiments we applied a voltage of 110 V which corresponds to an effective electrical field strength of 262 V cm^{-1}. Utilizing a 10 mM HEPES buffer at pH 7.5, fluorescein is negatively charged and accordingly deflected to the anode while rhodamine 6G is cationic and migrates to the cathodic side. At a pH of 7.5 rhodamine B is uncharged and not affected electrophoretically

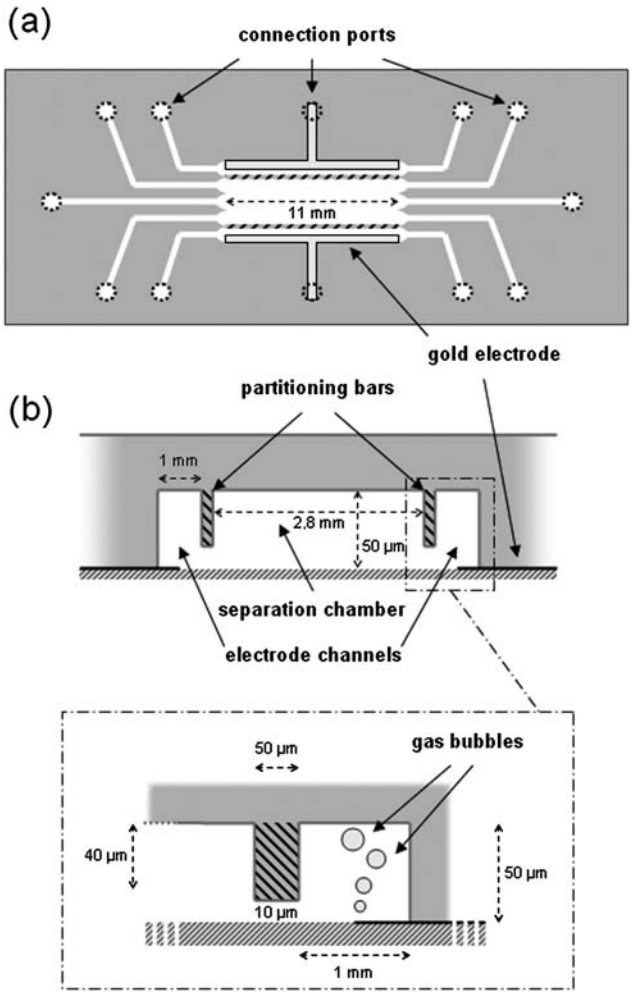

Fig. 4 Illustration of the chip design and bubble withheld principle. (a) Topview with channel structure and connection ports. (b) Cross-section of the separation area showing separation bed and electrode channels separated by the monolithic partitioning bars.

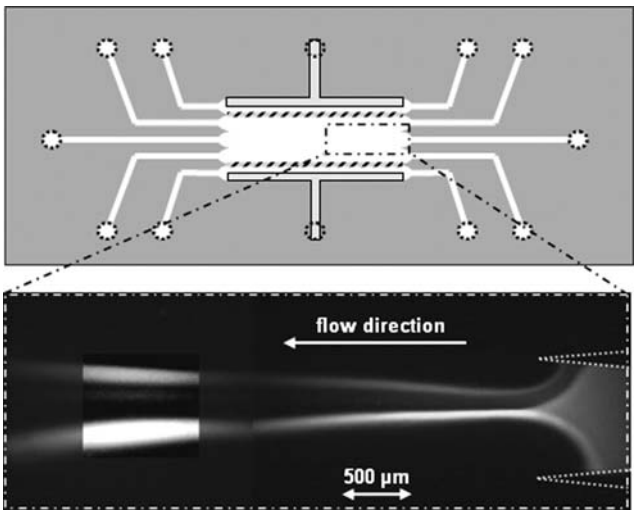

Fig. 5 Free-flow zone electrophoresis of fluorescein (lower stream), rhodamine B (center stream) and rhodamine 6G (upper stream), each 300 μg ml^{-1}, in aqueous 10 mM HEPES (pH 7.5), 0.2% HPMC and 0.1% Tween 20 with a linear flow velocity in the separation chamber of 5 mm s^{-1}. 110 V applied separation voltage, corresponding electrical field strength 262 V cm^{-1}. Picture merged from two microscopic photographs. Section with subsequently amplified contrast shows the weak fluorescent band of rhodamine B in the center position.

by the electrical field and can accordingly be used as a marker for the electroosmotic flow. Just after the voltage is switched on, the separation becomes visible. We determined the electrophoretic mobilities according to eqn (1) and compared these data with those from preceding CE experiments.

In general the obtained mobility data from μFFE experiments were in good agreement with those from capillary electrophoresis runs. For fluorescein we obtained electrophoretic mobilities of $(-2.8 \pm 0.1) \times 10^{-4}$ cm^2 s^{-1} V^{-1} in μFFE experiments and $(-2.9 \pm 0.1) \times 10^{-4}$ cm^2 s^{-1} V^{-1} in CE measurements. Since no electrophoretic deflection of rhodamine B could be observed, the EOF mobility in the chip can be determined to be less than 0.2×10^{-4} cm^2 s^{-1} V^{-1} which proves that EOF is effectively suppressed by the dynamic coating with HPMC.

Another fluorescent dye mixture consisting of rhodamine 116, fluorescein and rhodamine 6G could be separated with an only slightly changed electrolyte composition. In order to facilitate fluorescence imaging the dye concentrations were adjusted to gain comparable intensities. Using a multi-color fluorescence filter the separation results in three differently colored bands (see ESI†). When the FITC filter set with higher transmissions is used, five separated bands are detected. These five signals for three compounds can be explained by impurities of rhodamine 116 which yields three discrete signals in μFFE as well as in additional capillary electrophoretic separations. In these experiments we could apply voltages of up to 297 V, resulting in maximum field strength of 708 V cm^{-1}. In Fig. 6a the effect of the field strength on the dye separation is illustrated. The single electropherograms were obtained by line scan image evaluation at 75% of the separation chamber length. Arrows indicate the positions of the fluorescein and rhodamine 116 peaks. The corresponding resolution is given below the respective applied field strength. Baseline separation ($R > 1.5$) could be achieved at 332 V cm^{-1} with an associated separation voltage of 139 V (data calculated from linear regression). A corresponding photograph of a separation at 625 V cm^{-1} showing the five analyte signals of fluorescein, rhodamine 116 impurity A, rhodamine 116 impurity B, rhodamine 116 and rhodamine 6G from left to right is shown in Fig. 6b.

As we could prove that our device works well for dye mixtures we evaluated the applicability of μFFE to the separation of more demanding and less artificial applications. We applied the setup for the separation of small biomolecules such as amines and amino acids. The analytes were labeled with fluorescein isothiocyanate (FITC) for fluorescence detection. The experiments were performed with sample mixtures containing labeled glycine, tryptophan, aspartic acid, 2-butylamine, 2-octylamine and metoprolol. In Fig. 7 the separations of two different mixtures consisting of FITC–octylamine and FITC–aspartic acid (Fig. 7a) and FITC–butylamine, FITC–glycine and FITC–aspartic acid (Fig. 7b) are shown. Compared to the dye separations the separation of the labeled analytes into distinct zones occurs at much lower field strengths which can be explained by rather high individual electrophoretic mobilities. Due to the quite simple imaging setup using a common consumer camera, contrast and quality and the imaged area are far from optimum. However, these data show that the presented μFFE device is also applicable to less artificial applications like the common separations of fluorescent dyes found in μFFE publications. We are currently working on an improved optical detection scheme using a custom-built laser scanner which should enable imaging of large areas with high sensitivity.

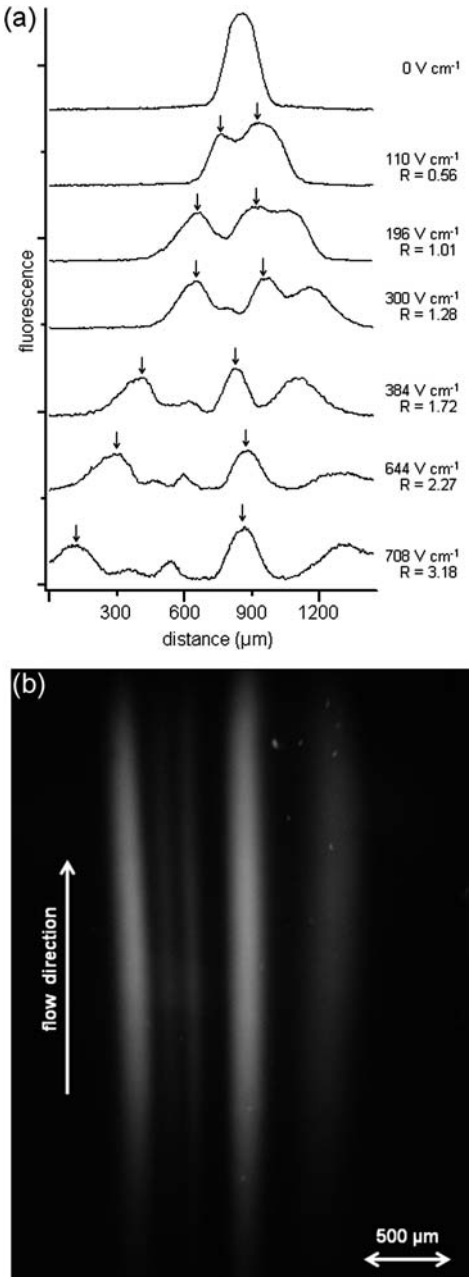

Fig. 6 FFZE of fluorescein, rhodamine 116 including impurities and rhodamine 6G in 10 mM HEPES in diluted methanol, 0.2% HPMC, 0.1% Tween 20. Analyte sequence from left to right: fluorescein, rhodamine 116 impurity A, rhodamine 116 impurity B, rhodamine 116, rhodamine 6G. (a) Splitting of the analytes and resolution trend of fluorescein and rhodamine 116 plotted against separation field strength. (b) Separated analytes at 262 V applied separation voltage (625 V cm^{-1}).

Conclusion

We have demonstrated the performance of a new miniaturized free-flow electrophoresis device with monolithic partitioning bars enabling bubble free μFFE separations. The three layer

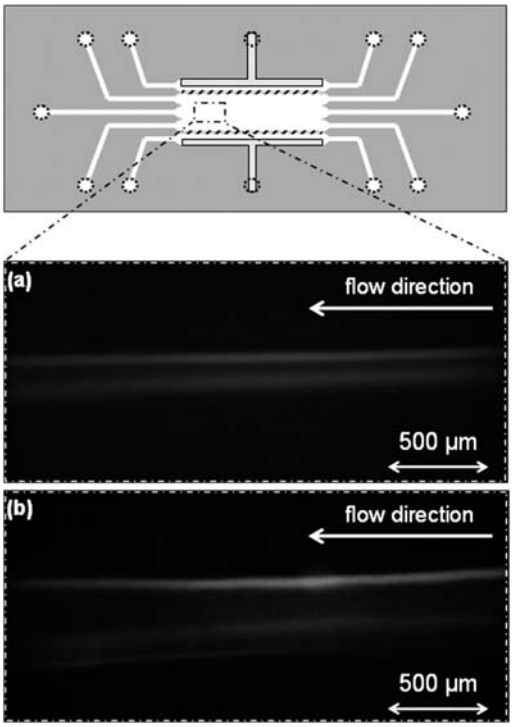

Fig. 7 FFZE of FITC-labeled biomolecules: (a) FITC–octylamine (upper stream) and FITC–aspartic acid (lower stream), each 5 mg ml^{-1}, in 20 mM CHES (pH 8), 0.2% HPMC, 0.1% Tween 20. Applied separation voltage 40 V and the corresponding electrical field strength 95 V cm^{-1}. (b) FITC–butylamine (10 mg ml^{-1}, upper stream), FITC–glycine (5 mg ml^{-1}, center stream) and FITC–aspartic acid (5 mg ml^{-1}, lower stream) in aqueous 5 mM borate buffer (pH 8), 0.2% PVP, 0.1% Tween 20. Applied separation voltage 44 V and the corresponding electrical field strength 105 V cm^{-1}.

sandwich chip is fabricated by softlithographic PDMS casting, allowing for straightforward manufacturing of the microfluidic device. Disturbing gas bubbles produced by electrolysis are restrained from entering the separation area by integrated partitioning bars. This enables µFFE experiments of high stability by avoiding the usual disturbance from generated gas bubbles. The µFFE chip was successfully applied to the separation of fluorescent dyes and fluorescently labeled amines and amino acids at separation field strengths of up to 708 V cm^{-1}. A current challenge is the sensitive detection and imaging of the rather big separation area. With this PDMS device as prototype we could prove the working principle of the new layout which can now be applied for the production of injection molded chips.

Acknowledgements

Funding for this research was provided by the German Federal Ministry of Education and Research (grant no. 01RI0643B). We would like to acknowledge the kind support by all partners of the joint project. Furthermore, thanks to Holger Hochmuth and Hannes Mönch for the preparation of the gold sputtered electrodes.

References

1 D. Kohlheyer, J. C. T. Eijkel, A. van den Berg and R. B. M. Schasfoort, *Electrophoresis*, 2008, **29**, 977–993.
2 N. Pamme, *Lab Chip*, 2007, **7**, 1644–1659.
3 D. Belder, *Angew. Chem., Int. Ed.*, 2009, **48**, 3736–3737.
4 G. M. Whitesides, *Nature*, 2006, **442**, 368–373.
5 A. J. deMello, *Nature*, 2006, **442**, 394–402.
6 D. Mark, S. Haeberle, G. Roth, F. von Stetten and R. Zengerle, *Chem. Soc. Rev.*, 2010, **39**, 1153–1182.
7 A. van den Berg and T. S. J. Lammerink, *Top. Curr. Chem.*, 1998, **194**, 21–49.
8 D. Janasek, J. Franzke and A. Manz, *Nature*, 2006, **442**, 374–380.
9 A. Chartogne, U. R. Tjaden and J. van der Greef, *Rapid Commun. Mass Spectrom.*, 2000, **14**, 1269–1274.
10 D. E. Raymond, A. Manz and H. M. Widmer, *Anal. Chem.*, 1994, **66**, 2858–2865.
11 D. E. Raymond, A. Manz and H. M. Widmer, *Anal. Chem.*, 1996, **68**, 2515–2522.
12 C.-X. Zhang and A. Manz, *Anal. Chem.*, 2003, **75**, 5759–5766.
13 B. R. Fonslow and M. T. Bowser, *Anal. Chem.*, 2005, **77**, 5706–5710.
14 D. Janasek, M. Schilling, J. Franzke and A. Manz, *Anal. Chem.*, 2006, **78**, 3815–3819.
15 Y. S. Huh, T. J. Park, K. Yang, E. Z. Lee, Y. K. Hong, S. Y. Lee, D. H. Kim and W. H. Hong, *Ultramicroscopy*, 2008, **108**, 1365–1370.
16 D. Kohlheyer, G. A. J. Besselink, S. Schlautmann and R. B. M. Schasfoort, *Lab Chip*, 2006, **6**, 374–380.
17 D. Kohlheyer, J. C. T. Eijkel, S. Schlautmann, A. van den Berg and R. B. M. Schasfoort, *Anal. Chem.*, 2007, **79**, 8190–8198.
18 J. W. Albrecht and K. F. Jensen, *Electrophoresis*, 2006, **27**, 4960–4969.
19 J. W. Albrecht, J. El-Ali and K. F. Jensen, *Anal. Chem.*, 2007, **79**, 9364–9371.
20 B. R. Fonslow, V. H. Barocas and M. T. Bowser, *Anal. Chem.*, 2006, **78**, 5369–5374.
21 B. R. Fonslow and M. T. Bowser, *Anal. Chem.*, 2008, **80**, 3182–3189.
22 V. Kostal, B. R. Fonslow, E. A. Arriaga and M. T. Bowser, *Anal. Chem.*, 2009, **81**, 9267–9273.
23 H. Kobayashi, K. Shimamura, T. Akaida, K. Sakano, N. Tajima, J. Funazaki, H. Suzuki and E. Shinohara, *J. Chromatogr., A*, 2003, **990**, 169–178.
24 Y.-A. Song, M. Chan, C. Celio, S. R. Tannenbaum, J. S. Wishnok and J. Han, *Anal. Chem.*, 2010, **82**, 2317–2325.
25 D. Janasek, M. Schilling, A. Manz and J. Franzke, *Lab Chip*, 2006, **6**, 710–713.
26 H. Lu, S. Gaudet, M. A. Schmidt and K. F. Jensen, *Anal. Chem.*, 2004, **76**, 5705–5712.
27 E. Shinohara, N. Tajima, H. Suzuki and J. Funazaki, *Anal. Sci.*, 2001, **17**, i441–i443.
28 D. Kohlheyer, J. C. T. Eijkel, S. Schlautmann, A. van den Berg and R. B. M. Schasfoort, *Anal. Chem.*, 2008, **80**, 4111–4118.
29 D. Belder, A. Deege, M. Maass and M. Ludwig, *Electrophoresis*, 2002, **23**, 2355–2361.
30 F.-U. Gast, P. S. Dittrich, P. Schwille, M. Weigel, M. Mertig, J. Opitz, U. Queitsch, S. Diez, B. Lincoln, F. Wottawah, S. Schinkinger, J. Guck, J. Käs, J. Smolinski, K. Salchert, C. Werner, C. Duschl, M. S. Jäger, K. Uhlig, P. Geggier and S. Howitz, *Microfluid. Nanofluid.*, 2006, **2**, 21–36.
31 L. Gitlin, P. Schulze and D. Belder, *Lab Chip*, 2009, **9**, 3000–3002.

